Sulfur, Not Too Far Behind O, N, and C: SH···π Hydrogen Bond

Himansu S. Biswal[†] **and Sanjay Wategaonkar***

Department of Chemical Sciences, Tata Institute of Fundamental Research, Homi Bhabha Road, Colaba, Mumbai 400 005

Received: August 11, 2009; Revised Manuscript Received: September 24, 2009

We report hydrogen-bonded complexes of H_2S with indole and 3-methyl indole stabilized by the S−H···π interaction. It is interesting to discover that although sulfur and its hydrides are known as poor hydrogen-bond donor/acceptors, sulfur is not too far behind oxygen, nitrogen, and carbon in regard to forming the π-type hydrogen bonds. This report also extends the scope of our earlier studies from σ-type hydrogen-bonded complexes of sulfur (O−H···S and N−H···S σ-type hydrogen-bonded complexes) to π-type hydrogen-bonded complexes of sulfur (S−H···π π-type hydrogen-bonded complexes). The experiments were carried out using the supersonic jet expansion technique, and the complexes were probed using laser-induced spectroscopy such as laser-induced fluorescence (LIF), resonant two-photon inonization (R2PI), and fluorescence dip infrared spectroscopy (FDIRS). The FDIR spectroscopy revealed that while there was no shift in the N−H stretch, the S−H stretch was red shifted by about 21 cm^{-1}. For the H_2O complexes of indole and 3-methylindole, however, there was a significant red shift in the N−H stretch. These observations suggest that H_2O forms a NH···O type complex, whereas H_2S prefers to form a SH···π type complex. The experimental results were complemented by ab initio calculations and energy decomposition analysis. The binding energies for both the σ-type and π-type hydrogen-bonded M·L complexes (M = indole and 3-methylindole; L = H_2O and H_2S) were calculated by extrapolating MP2 interaction energies to the complete basis set limit. The calculated M·H_2S (σ-type) interaction energy (2.74 kcal/mol) was considerably smaller than that of the M·H_2S π-type hydrogen-bonded complex (4.89 kcal/mol), which is exactly opposite of the trend found for the M·H_2O complexes. This is consistent with the experimental observations. Comparison of the S−H···π interaction with the other type of X−H···π (X = C, N, and O) shows that the S−H···π interaction is the strongest among them. In all of the π-type HB complexes, the dispersion energy component has significant contribution to the total binding energy.

1. Introduction

The 90s saw quite a few interesting results in regard to the hydrogen-bonding interactions involving a hydrogen atom covalently bonded to some atom and aromatic π-electron density.[1−10] These were termed as π-type hydrogen bonds. The conventional definition of a X−H···Y hydrogen bond had already been expanded[11] to include Y as an "electron-rich atom or group of atoms" rather than just another "electronegative atom". A few celebrated examples of the π-type hydrogen bonds include benzene·H_2O,[1−5,10,12−16] benzene·CH_3OH,[14,17] benzene·NH_3,[6,7,16,18−22] benzene·$CHCl_3$,[9,23−25] benzene·hydrogen halide,[8,26,27] and benzene dimer complexes.[28−42] In each case, it was shown that one of the XH bonds of the hydrogen-bond-donating moiety points toward the aromatic ring and the XH stretching frequency, except in the case of the C−H···Y interaction, which exhibits a red shift that is a hallmark characteristic of a hydrogen bond. Further, these hydrogen bonds are much weaker than the conventional X−H···Y σ-type hydrogen bonds. The benzene·water and benzene·ammonia complexes were shown to be very floppy, with the barrier height for the hindered rotation around the C_2 and C_3 axis of H_2O and NH_3, respectively, being very low.[3,6,7,22,43]

In this work, we present experimental evidence of the S−H···π interaction in indole·H_2S and 3-methylindole·H_2S complexes. Experimental techniques like LIF and FDIR spectroscopy and ab intio calculations were used to show that H_2S preferentially forms a π-type HB, although the possibility of forming a N−H···S σ-type hydrogen-bonded complex existed in these systems. The importance of S−H···π as well as S···π interaction is evident from the structures of the proteins and biomolecules.[44−49] There have been a few reports in the literature where some efforts have been made to characterize the S−H···π hydrogen bonds computationally.[46,50−54] However, the experimental investigations of the S−H···π HB under isolated jet-cooled conditions have been very sparse. Only one report on S−H···π interaction exists where the interaction between H_2S and benzene was addressed using FT-microwave rotational spectroscopy.[43] The data indicated that H_2S was located on the C_6 axis of the C_6H_6 with the center of mass (C_6H_6)−S distance of 3.818 Å. The angle between the C_6 axis of C_6H_6 and the C_{2v} axis of H_2S was determined to be 28.5° in the complex.

We have recently published a detailed comparative study of hydrogen-bonding interactions between *p*-cresol and the H_2S/H_2O system.[55] It was shown that both H_2O and H_2S form O−H···O/S σ-type hydrogen-bonded complexes. The O−H···S hydrogen bond was found to be weaker than the O−H···O HB and had a major contribution from the dispersion energy component compared to that in the O−H···O interaction. The results presented here are in stark contrast with those reported in the case of *p*-cresol complexes. It is well established that H_2O forms a σ-type HB with indole (IND) and 3-methylindole (3-MI).[56−59] It has also been reported that H_2O forms a π-type

* To whom correspondence should be addressed. Phone: 91-22-2278-2259. Fax: 91-22-2278-2106. E-mail: sanwat@tifr.res.in.
† E-mail: himansu@tifr.res.in.

10.1021/jp907747w CCC: $40.75
Published on Web 10/15/2009

HB in the case of the 1-methylindole complex[60] where the NH binding site is blocked by the methyl group. Therefore, all of the experimental as well as the computational results for H_2S have been compared with the corresponding H_2O complexes. Attempts are made to rationalize the difference in hydrogen-bonding characteristics of H_2O and H_2S. The results for the S−H···π HB are also compared with the other X−H···π (X = C, N, and O) HB systems, and it was shown that the SH···π HB was the strongest among all of them and that it was completely stabilized by the dispersion interaction.

2. Experimental Details

The details of the experimental approach can be found elsewhere.[55,61,62] In brief, the hydrogen-bonded complexes were formed using the supersonic jet expansion method and investigated by means of laser-induced fluorescence (LIF) and fluorescence dip infrared spectroscopy (FDIRS). All of the experiments were carried out using 10 Hz Nd^{3+}:YAG-pumped dye lasers. For the FDIRS experiments, typical pulse energies were 10−20 μJ for the excitation laser and ∼1 mJ for the IR laser. Both of the lasers were temporally synchronized using a delay generator (SRS-DG 535).

FDIRS was used to probe the changes in the X−H vibrational (X = C, N, O, S) frequencies in the hydrogen-bonded complexes. In this technique, jet-cooled molecules or complexes are excited to a specific vibrational level by a tunable IR laser. The depletion of the $v = 0$ level population induced by the vibrational excitation is monitored by means of LIF using a UV laser. The delay time between the IR laser and the UV probe laser is nominally set to 50−100 ns. The UV laser frequency is tuned to a vibronic band, usually the band origin of the species being probed, and the total fluorescence is monitored. Thus, a fluorescence dip vibrational spectrum is obtained by scanning the tunable IR laser while monitoring the fluorescence signal.

The tunable IR covering the C−H, N−H, O−H, and S−H stretching frequency range (1.8 to 4.0 μm) was generated by the difference frequency mixing method. The second harmonic (532 nm) of a ∼10 ns, 10 Hz repetition rate Nd^{3+}:YAG laser (Quanta-Ray PRO 230-10) was used to pump a SIRAH dye laser (Sirah, CSTR LG 18) whose output was mixed with the fundamental of the Nd^{3+}:YAG laser (1064 nm) in a $LiNbO_3$ crystal. Styryl-8 dye in DMSO was used for the wavelength range of ∼760−800 nm, while styryl-9 dye in ethanol was used for the wavelength range of ∼795−840 nm. The laser system was coupled with the SIRAH autotracker unit for continuous wavelength scan. The resultant IR output was separated from the 1064 nm input and dye laser fundamental using appropriate dichroic filters.

The reagents indole, 3-methylindole, and benzene were purchased from Sigma−Aldrich and used without further purification. Indole and 3-methylindole were heated to ∼60−80 °C to generate sufficient vapor pressure to record the spectra with good *S/N* ratio. Hydrogen sulfide (∼99% pure) was purchased from a local commercial source. Helium obtained from local commercial sources was used without further purification as the buffer gas. The buffer gas was flowed over a reagent bottle containing H_2O to synthesize the M·H_2O complexes. The optimum amount of H_2O for generating the 1:1 complexes was maintained by means of a needle valve. A 2−5% premix of H_2S in helium was used to generate a 1:1 complex of M·H_2S complexes.

3. Computational Details

The geometry optimizations and frequency calculations were carried out using the Gaussian 03 program.[63] Three-dimensional pictures of the complexes were rendered using ChemCraft (trial version).[64] The interaction or binding energies for all of the complexes were calculated after applying the zero-point energy (ZPE), the basis set superposition error (BSSE), and the fragment relaxation energy corrections to the total binding energy. The MP2 level interaction energies were calculated using aug-cc-pVXZ (X = D and T) basis sets. The interaction energies at the basis set limit were then estimated using the two-point extrapolation formula of Helgaker et al.[65] To evaluate the direction and magnitude of the donor−acceptor interactions, the natural bond orbital (NBO)[66−68] analysis for all of the complexes was performed using the NBO 5.0 program.[69] The interaction energies of the complexes were decomposed at the HF/aug-cc-pVDZ theory level into physically meaningful individual energy components[70] using the reduced variational space self-consistent field (RVS)[71] decomposition analysis. The RVS decomposition analysis was performed using the Gordon and Chen[72] algorithm in the GAMESS, U.S.A.[73]

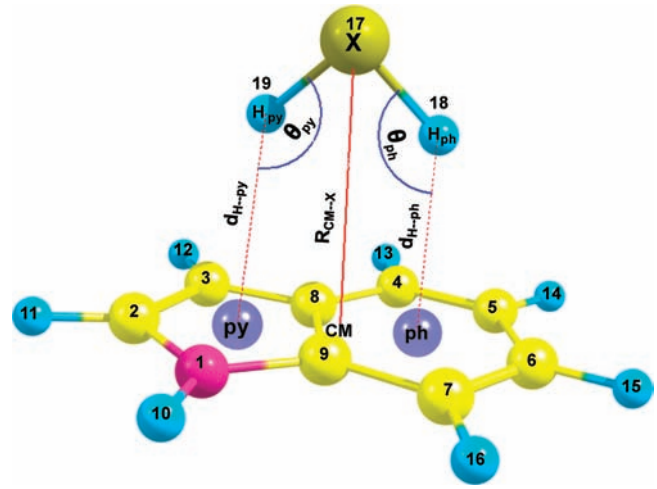

Figure 1. MP2/aug-cc-pVDZ optimized structure of the indole·H_2S (π) complex. The atom numbering is employed to define the structural parameters; see text and Table 1.

4. Results and Discussion

4.1. Equilibrium Geometry and Interaction Energy. The geometry optimizations for the monomers and complexes were done at the MP2 level of theory with the aug-cc-pVDZ basis set followed by the frequency calculations to ensure that all of the structures were the true minima. Both the σ-type and π-type HB complexes of H_2O and H_2S with IND and 3-MI were optimized. The structural parameters used to define the hydrogen-bonded structures of the π-type complexes are shown in Figure 1. All of the geometrical parameters such as the $d_{H\cdots ph}$ and $d_{H\cdots py}$ (ph and py indicates the centroid of phenyl and pyrrole rings of indole), R_{CM-X} (CM indicates the center of mass of indole, X = O or S), Δr_{X-H}, and the H-bond angles θ_{ph} and θ_{py} are listed in Table 1. It also gives $d_{H\cdots Y}$ (Y = O or S), $R_{N\cdots Y}$, Δr_{NH}, and ∠NHY for the σ-type complexes. For the σ-type HB complexes, the hydrogen bond angle (θ) was 158 and 178° for N−H···S and N−H···O hydrogen-bonded complexes, respectively, while θ_{ph} and θ_{py} angles were comparable for both S−H···π and O−H···π HB complexes, namely, 135 and 131° versus 129 and 130°, respectively. The increase in the X−H bond length, that is, the N−H bond length in the M·H_2O (σ) complexes, was higher than that in the M·H_2S (σ) complexes, but for the π-type complexes, the trend was exactly opposite, that is, the S−H bond lengths increased more than the O−H

TABLE 1: Ab Initio Calculated Structural Parameters and Binding Energy of Indole·L and 3-MI·L (L = H_2O and H_2S) σ- and π-Type Hydrogen-Bonded Complexes Using the MP2/aug-cc-pVDZ Method

	indole·L				3-methyl indole·L			
parameters	H_2O (π)	H_2O (σ)	H_2S (π)	H_2S (σ)	H_2O (π)	H_2O (σ)	H_2S (π)	H_2S (σ)
$d_{H\cdots ph}/d_{H\cdots Y}$ (Å)	2.766	1.943	2.431	2.541	3.074	1.949	2.517	2.545
$d_{H\cdots py}$ (Å)	2.495		2.487		2.310		2.410	
$R_{CM\cdots X}/R_{N\cdots Y}$ (Å)	3.145	2.962	3.385	3.507	3.269	2.967	3.379	3.506
$\Delta r_{X-H}/\Delta r_{N-H}$ (Å)	0.0030	0.0069	0.0045	0.0047	0.0032	0.0067	0.0049	0.0045
$\theta_{ph}/\angle$NHY (deg)	129.5	178.3	134.7	158.4	120.7	178.1	135.1	157.6
θ_{py} (deg)	130.1		131.3		142.0		133.5	
ΔE_0^{CBS} (kcal/mol)	−3.57	−4.53 (−4.67)[a]	−4.89	−2.74	−3.83	−4.35 (−4.49)[b]	−5.17	−2.66

[a] Experimental binding energy of IND·H_2O; ref 75. [b] Experimental binding energy of 3-MI·H_2O; ref 59.

bond lengths. If the inverse relation between Δr_{X-H} of the hydrogen bond donor and its strength is invoked, then it can be inferred that the N−H group forms a stronger σ-type HB with H_2O compared to that with H_2S, while H_2S forms stronger π-type HB complexes relative to those formed by H_2O.

The interaction energies for the complexes were calculated at the MP2 level of theory. Various energy corrections like basis set superposition error (ΔE_{BSSE}), deformation or relaxation energy (ΔE_{Relax}), and zero-point energy correction (ΔZPE) were applied to get the corrected interaction energy (ΔE_0). According to the NIST computational chemistry comparison and benchmark database,[74] a scaling factor of 0.959 was used to scale the ZPE computed at the MP2/aug-cc-pVDZ level of theory. Single-point energy calculations were done at the MP2/aug-cc-pVTZ level of theory for the MP2/aug-cc-pVDZ optimized structures. The interaction energies at the complete basis set (CBS) limit for the MP2/aug-cc-pVDZ optimized structures were estimated using the two-point extrapolation formula of Helgaker et al.[65]

$$E^{CBS} \approx \frac{X^3E(X) - (X-1)^3E(X-1)}{X^3 - (X-1)^3} \qquad X = 3 \text{ for the aug-cc-pVTZ basis set} \quad (1)$$

The ZPE- and deformation-energy-corrected complete basis set interaction energy (ΔE_0^{CBS}) is provided in the last row of Table 1. The corrected binding energies of IND·H_2O and 3-MI·H_2O were 4.53 and 4.35 kcal/mol, respectively, which are about 97% of the experimentally determined binding energy.[59,75] This shows that the binding energies obtained using this level of computation are acceptable. It can be seen from the table that in the case of H_2O complexes, the binding energies of the σ-type complexes are greater than those of the π-type, whereas for the H_2S complexes, the trend is opposite. Further, while the binding energies for the M·H_2O (σ) complexes were marginally higher than those for the M·H_2O (π) complexes, those for the M·H_2S (σ) complexes were almost half as much as those for the M·H_2S (π) complexes. This is consistent with the earlier inference based on the geometrical parameters that H_2O forms stronger σ-type HB complexes while H_2S forms stronger π-type HB complexes. On an absolute level, the binding energies for the M·H_2S (π) complexes were even higher than those for the M·H_2O (σ) complexes, suggesting that in this particular case, the π-type complexes are actually stronger than the σ-type HB complexes, contrary to the known trend. The increase in the S−H bond lengths and binding energy for the 3-MI·H_2S (π) complex were higher than those of the IND·H_2S (π) complex.

4.2. Electronic Spectroscopy. Figure 2 shows the mass spectra of the M·H_2S complexes recorded using a 2% H_2S mixture in helium buffer gas. The 1c-R2PI spectra of M·H_2S complexes could not recorded due to very poor signal in the complex mass channel perhaps due to the prompt dissociation of the complex upon ionization. Figure 3 displays the LIF spectra of indole (IND) in the absence (Figure 3a) and in the presence (Figure 3b) of H_2S, while Figure 3c and d displays those for 3-methylindole (3-MI), respectively. In all of the LIF spectra, features due to M·H_2O complex were always present due to residual water in the helium buffer gas. The $S_1 \leftarrow S_0$ band origins of IND, IND·H_2O, 3-MI, and 3-MI·H_2O were

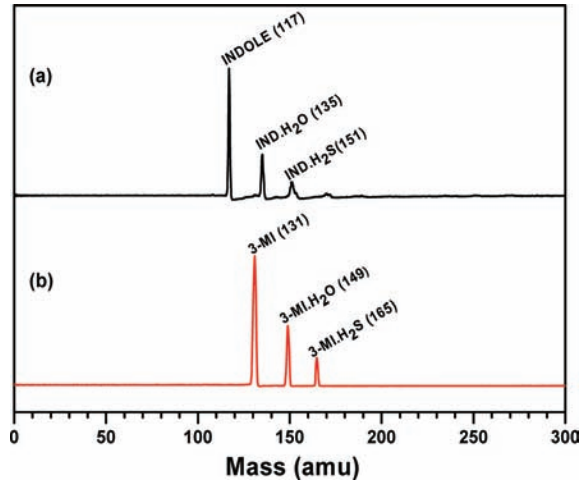

Figure 2. ToF mass spectrum in the presence of 2% H_2S. For indole, the laser frequency was 35197 cm^{-1}, while for 3-MI, it was 34811 cm^{-1}. The laser frequencies correspond to the band origins of the respective H_2S complexes.

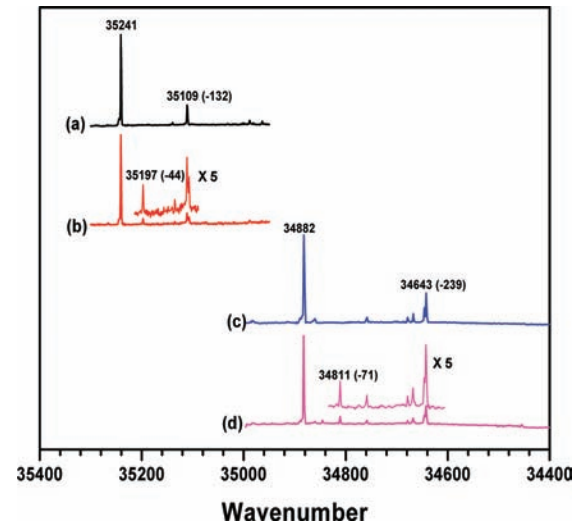

Figure 3. LIF spectra of (a) indole, (b) indole in the presence of 2% H_2S, (c) 3-methylindole, and (d) 3-methylindole in the presence of 2% H_2S.

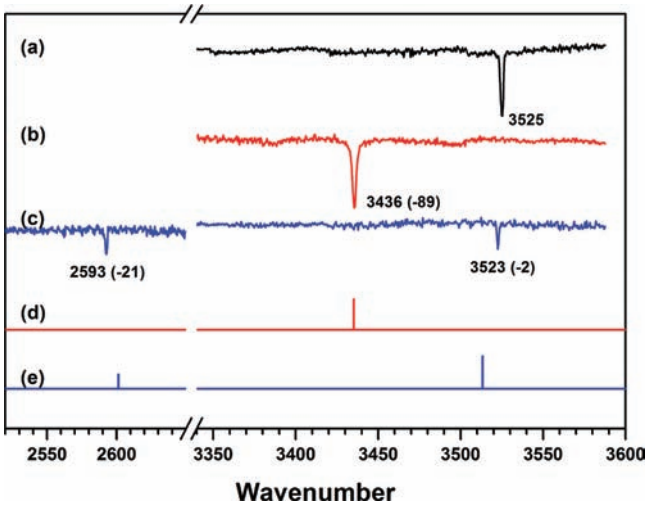

Figure 4. FDIR spectra of (a) indole, (b) IND·H_2O, and (c) IND·H_2S recorded while tuning the probe laser at the band origin of the respective species. Trace (c) also covers the S−H stretch region. Traces (d) and (e) show the computed IR spectra of the NH-bound and π-bound H_2S complex with indole, respectively.

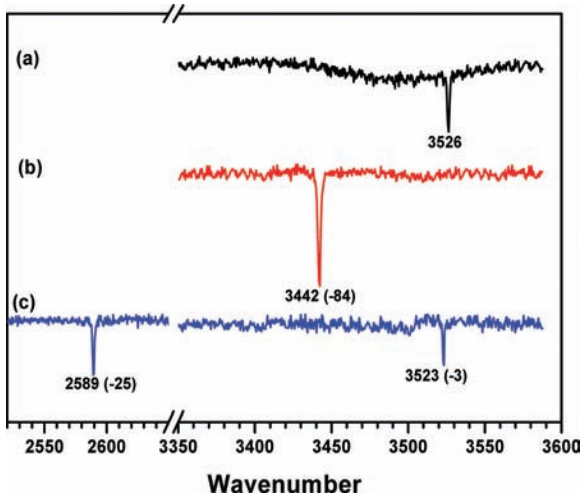

Figure 5. FDIR spectra of (a) 3-methylindole, (b) 3-MI·H_2O, and (c) 3-MI·H_2S recorded while tuning the probe laser at the band origin of the respective species. Trace (c) also covers the S−H stretch region.

observed at 35241, 35109, 34882, and 34643 cm^{-1}, respectively. In the presence of 2% H_2S, one extra prominent peak was observed at 35197 cm^{-1} in the IND spectrum (Figure 3b) and at 34811 cm^{-1} in the 3-MI spectrum (Figure 3d). These extra peaks were assigned as the band origins of the respective M·H_2S complexes. The red shift in the band origin of the IND·H_2S complex was 44 cm^{-1}, whereas that of the 3-MI·H_2S complex was 71 cm^{-1}. The red shifts in the band origins of IND·H_2S and 3-MI·H_2S complexes were much smaller compared to those of their respective H_2O complexes. The red shift in the band origin of IND·H_2S was however similar to that of the IND·CH_4 complex,[76] which has been shown to form a π-type HB.

4.3. Infrared Spectroscopy. The FDIR spectra of the monomers IND and 3-MI and their complexes with H_2O and H_2S in the N−H stretching frequency region are shown in Figures 4 and 5, respectively. In all cases, the excitation laser was fixed at the band origins of the respective complexes. The N−H stretching frequencies of the chromophores were substantially red shifted relative to the monomers in the M·H_2O complexes. However, in the case of M·H_2S complexes, there was hardly any shift in the N−H stretching frequency. The N−H

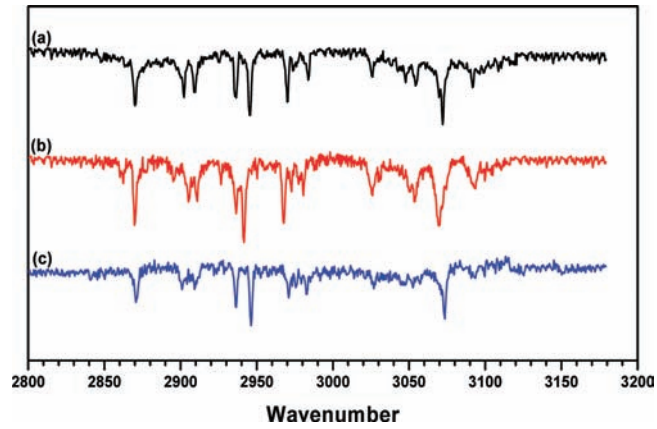

Figure 6. FDIR spectra of (a) 3-MI, (b) 3-MI·H_2O, and (c) 3-MI·H_2S in the C−H stretch region, recorded while tuning the probe laser at the band origin of the respective species.

stretch red shift was 89 cm^{-1} in the IND·H_2O complex, while it was barely 2 cm^{-1} for the IND·H_2S complex. Similarly, the red shift in the N−H stretch of the 3-MI·H_2O complex was 84 cm^{-1} as opposed to 3 cm^{-1} for the 3-MI·H_2S complex. This indicates that the N−H stretch is almost unperturbed in the M·H_2S complexes, and it can be safely deduced that the N−H bond is not involved in hydrogen bonding with H_2S.

The FDIR spectra in the S−H stretch region were recorded to see if there were any changes in the S−H frequencies of H_2S. The IR transition probabilities of SH oscillators are 2−3 orders of magnitude smaller compared to those OH and NH oscillators, and as such, the SH stretching transitions have never been reported for the complexes involving the SH bonds. Figures 4 and 5 show the FDIR spectra for the IND·H_2S and 3-MI·H_2S complexes in the S−H region. In each of the two spectra, a fluorescence dip was observed at 2593 and 2589 cm^{-1}, respectively. These were assigned to the symmetric S−H stretching mode based on the computational normal-mode analysis. Figure 4 also shows the computed IR spectra of the NH bound as well as the π-bound indole·H_2S complexes. The IR transition probability for the SH excitation in the π-bound complex increased considerably due to the hydrogen bonding. It can be seen that the observed spectrum is in good agreement with that of the π-bound indole·H_2S complex. The S−H stretch for IND·H_2S was red shifted by 21 cm^{-1}, while that for the 3-MI·H_2S was red shifted by 25 cm^{-1} with respect to the symmetric S−H stretch (2615 cm^{-1})[77,78] of the H_2S monomer. The observation of the SH stretching transition by itself and its red shift for both the complexes suggests that H_2S acts as a HB donor rather than a HB acceptor. Preferential population of only the π-bound H_2S complexes corroborates the estimated greater stability of the M·H_2S (π) complexes relative to M·H_2S (σ) complexes.

Figure 6 shows the FDIR spectra in the C−H stretch region for the 3-MI and its complexes with H_2O (Figure 6b) and H_2S (Figure 6c). The C−H stretches of the phenyl and pyrrole ring were broadened for 3-MI·H_2O, while those for the 3-MI·H_2S complex were identical to those of the 3-MI monomer. Broadening of spectral features has been reported for other σ-HB complexes of indole and 3-MI.[79] In the case of H_2O complexes, it has been attributed to the hindered rotation of the H_2O moiety around the N−H···O bond. Absence of such broadening in the case of the H_2S complex suggests that either the barrier for the rotation is too high if it is a N−H···S type hydrogen bond or that H_2S is not bound to the NH group at all. We prefer the latter possibility based on the other observations.

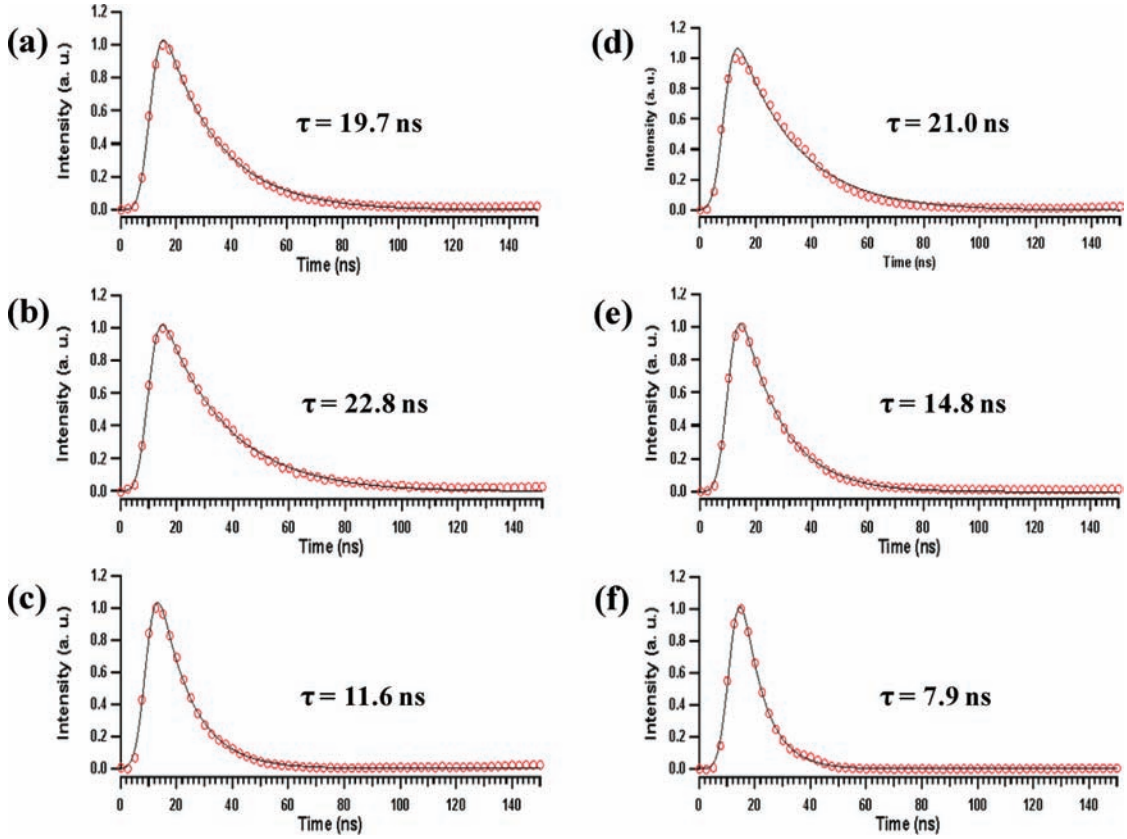

Figure 7. Fluorescent decay profiles of (a) IND, (b) IND·H_2O, (c) IND·H_2S, (d) 3-MI, (e) 3-MI·H_2O, and (f) 3-MI·H_2S for the (0,0) transition of the respective species.

TABLE 2: Experimentally Observed Parameters Such As XH Stretching Frequency Shift, The Band Origin Shift, The S_1 State Lifetime, and Binding Energy of Indole·L and 3-MI·L (L = H_2O and H_2S) σ- and π-Type Hydrogen-Bonded Complexes

complex	HB type	$\Delta\nu_{NH}$ (cm^{-1})	$\Delta\nu_{XH}$ $(cm^{-1})_{X=O,S}$	ΔE_{BO} (cm^{-1})	τ (ns)	ΔE_0 (kcal/mol)
IND·H_2O	N−H···O σ HB	–89	–5[a]	–132	22.8	–4.67[a]
IND·H_2S	S–H··· π π HB	–2	–21	–44	11.6	–4.89[b]
3-MI·H_2O	N–H···O σ HB	–84	–5[a]	–239	14.8	–4.49[a]
3-MI·H_2S	S–H··· π π HB	–3	–25	–71	7.9	–5.17[b]

[a] Experimental value from ref 57. [b] Binding energy computed at the CBS limit.

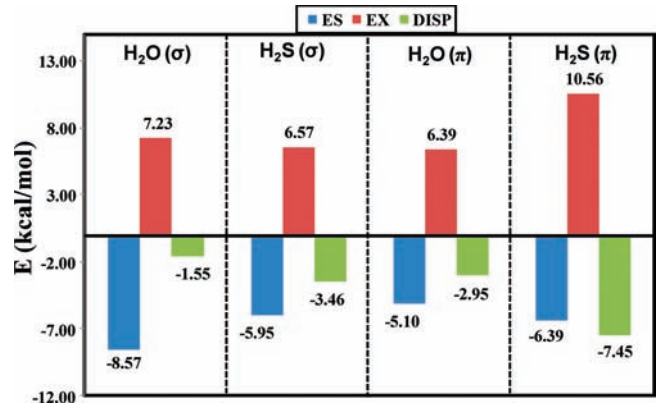

Figure 8. The electrostatic attraction (ES), exchange repulsion (EX), and dispersion energy (DISP) contributions obtained using RVS decomposition analysis for IND·H_2O (σ), IND·H_2O (π), IND·H_2S (σ), and IND·H_2S (π) complexes.

4.4. Lifetime Measurements. It is known that the photophysical properties of indole, such as the fluorescence quantum yield, radiative lifetime, an so forth, are very sensitive to the local environment. In fact, a lot of experimental investigations have been performed on indole and its complexes with different solvent molecules like H_2O, MeOH, NH_3, and benzene.[56−59,80−89] In all cases, the complexes were of the N−H···X σ-type HB complexes. Since in the indole-based chromophores the $S_1 \leftarrow S_0$ elctronic transition is a $\pi^* \leftarrow \pi$ transition, it is expected that the change in the lifetime for the S_1 state will be more pronounced in the π-type HB complexes rather than that in σ-type HB complexes. The lifetime measurements for both the monomers and their complexes were carried out for the band origin excitation and fluorescence decay curves are provided in Figure 7. The lifetimes of the excited state were obtained by fitting the experimental data with a single exponential after deconvolution of the excitation pulse. The excited-state lifetimes for the IND, IND·H_2O, and IND·H_2S complexes were 19.7, 22.8, and 11.6 ns, respectively. The values for the IND and IND·H_2O complexes were within 10% of the reported values.[76,90−94] There was hardly any change in the S_1 state lifetime for the IND·H_2O complex, whereas in the case of the IND·H_2S complex, it shortened considerably. For 3-MI, the S_1 state lifetime was found to be 21 ns, while those for 3-MI·H_2O and 3-MI·H_2S were 14.8 and 7.9 ns, respectively. A substantial decrease in the lifetime of the M·H_2S complexes in both cases shows that the S_1 state decay mechanisms in these complexes are quite different than those associated with the σ-type complexes. At this stage, it is difficult to say whether it is due to the increased mixing of the L_a and L_b states or an intrinsic increase in the radiative transition probability which is respon-

TABLE 3: Comparison of Computed Structural Parameters and the Binding Energy of IND·L (L = H_2O, H_2S, NH_3, and CH_4) π-Type HB Complexes with Experimental Values for the Benzene·L π-Type HB Complexes

	indole·L (π) (theoretical)				benzene·L (π) (experimental)			
parameters	H_2O[a]	H_2S	NH_3	CH_4	H_2O	H_2S	NH_3	CH_4
$R_{CM\cdots X}$ (Å)	3.145	3.385	3.198	3.186	3.411[b]	3.818[c]	3.590[d]	3.800[e,f]
$\Delta\nu$ (cm^{-1})	48.0 (42.0)[g]	45.0 (21.0)[h]	20.0	19.0	23.0[i]	n/a[q]	8.3[j]	5.0[k]
ΔE_0^{CBS} (kcal/mol)	−3.57 (4.10)[l]	−4.89	−2.56	−2.01	−2.44[m]	−2.81[e,n]	−1.84[o]	−1.13[p]

[a] Values in the parentheses are for the 1-methylindole·H_2O complex. [b] Reference 3. [c] Reference 43. [d] Reference 6. [e] Reference 97. [f] Values for benzene·CH_4 and benzene·H_2S complexes computed at the CCSD(T)/CBS level. [g] Reference 57. [h] Experimental value determined in this work. [i] Reference 12. [j] Reference 21. [k] Reference 95. [l] Reference 60. [m] Reference 2. [n] Reference 51. [o] Reference 19. [p] Reference 96. [q] n/a: not available.

TABLE 4: RVS Energy Decomposition Analysis for IND·L (X−H···π Hydrogen-Bonded) Complexes (L = H_2O, H_2S, NH_3, and CH_4)

complex	ΔE_{CT}	ΔE_{ES}	ΔE_{PL}	ΔE_{EX}	ΔE_{BSSE}	ΔE_{HIGH}	ΔE_{INT}	ΔE_{INT}^{BSSE}	ΔE_{MP2}^{BSSE}	ΔE_{Disp}
IND·H_2O	–0.64	–5.95	–0.83	6.57	0.52	–0.07	–1.44	–0.92	–4.38	–3.46
IND·H_2S	–1.05	–6.39	–0.81	10.56	0.67	–0.08	1.56	2.23	–5.22	–7.45
IND·NH_3	–0.43	–3.77	–0.44	6.18	0.64	–0.03	0.87	1.51	–2.99	–4.50
IND·CH_4	–0.41	–2.56	–0.34	6.50	0.73	0.01	2.47	3.20	–2.29	–5.49

sible for the reduction in the lifetimes of these complexes. All of the lifetime values along with the binding energies of the complexes are summarized in Table 2.

4.5. Interaction Energy Decomposition. The experimental results suggest that H_2S forms a π-type HB, while H_2O forms a σ-type HB. Computed binding energies also support the π-type in the case of H_2S, and in the case of H_2O, the σ-type H-bonded structure is relatively stable. It is also important to know the type of interaction that dominates in each of the two cases, that is, π-type hydrogen bonding versus the σ-type hydrogen bonding. To better understand the nature and extent of different forces contributing to the intermolecular attraction in these complexes, individual energy components [electrostatic (ES), polarization (PL), charge transfer (CT), and exchange (EX)] of the total interaction energy were obtained using the reduced variational space self-consistent field (RVS)[71] method. The correlation energy or the dispersion energy (DISP) was calculated as the difference between the BSSE-corrected total interaction energy computed at the MP2 level and that computed using the RVS procedure. All of the calculations were done using the aug-cc-pVDZ basis set. The major components like ES, EX, and DISP for both the σ- and π-type HB complexes are shown in Figure 8. In the case of H_2O complexes, regardless of the type of H-bond, the electrostatic component is the major attractive component of the total interaction energy, while for the H_2S complexes, the dominant component depends upon the type of H-bond, that is, for the σ-type, it is the electrostatic, whereas for the π-type, it is dispersion. For the IND·H_2S (π) complex, all three components, namely, the electrostatic attraction (ES), exchange repulsion (EX), and the dispersion stabilization, are all greater than those for the IND·H_2O (π) complex. A similar trend has also been reported for the naphthalene·L and azulene·L (L = H_2O, H_2S) complexes using SAPT (DFT) energy decomposition analysis.[53,54]

4.6. Comparison of S−H···π HB with Other X−H···π HBs, (X = C, N, and O). At this stage, it is imperative to compare the S−H···π interaction with other π-type HB complexes. The computations such as geometry optimization and frequency analysis were extended to include the other π-type IND·L (L = NH_3 and CH_4) complexes at the same level of theory. The interaction energies at the complete basis set (CBS) limit were also estimated as outlined earlier. All of these parameters are listed in Table 3. The computed binding energy for the IND·H_2O π-type complex was compared with the experimental value reported for the 1-methylindole·H_2O π-type complex.[60] It is in agreement with the trend that in the case of indole·H_2O complexes, the σ-type complex is more stable than the π-type complex. For the sake of completeness and comparison, the available experimental results for the benzene·L complexes[1,3,5,6,19,21,43,95−97] in regard to the binding energy (ΔE_0), red shift of the X−H stretch ($\Delta\nu$), and the distance from X to the center of mass of the aromatic ring ($R_{CM\cdots X}$) are also listed in Table 3. The most interesting feature that stands out in the comparison is that the S−H···π HB interaction energy is higher than any other π-type HB complexes. The interaction energies follow the order S−H···π > O−H···π > N−H···π > C−H···π.

Structurally, the H_2O and H_2S complexes were similar, that is, both of the hydrogens point toward the indole ring. The computed red shifts of the X−H stretch for the O−H···π and S−H···π were also very similar and almost two times that of the N−H···π and C−H···π interactions. The experimentally observed SH red shift was 21 cm^{-1}, which is incidentally of the same order as that of the OH red shift observed in the benzene·H_2O complex. Although the benzene·H_2S complex has not been investigated using the FDIRS, it has been studied using the FTMW (Fourier transform microwave) spectroscopy,[43] and the reported structure is similar to the one predicted here for the IND·H_2S complex. Therefore, one can expect a similar red shift in the SH stretch in the benzene·H_2S complex. The other parallel between the indole·L and benzene·L complexes is that the XH red shifts for the OH and SH are much larger than those observed for the NH and CH stretches. Fujii et al. have reported the red shift in the symmetric CH stretch in the benzene·CH_4 π-type complex as 5 cm^{-1}, which can be compared with the 21 cm^{-1} red shift in the OH stretch of the benzene·H_2O complex. The computed $R_{CM\cdots X}$ values for the IND·L complexes were smaller compared to the reported experimental values for the benzene·L complexes, suggesting that the former complexes are relatively more stable than the later.

The RVS energy decomposition analysis was carried out for all four aforementioned IND·L complexes, and the results are presented in Table 4. At the HF level, only the IND·H_2O complex was stable. The numbers presented in Table 4 suggest that only the electrostatic forces are not sufficient to stabilize the X-H···π HB complexes. The dispersion energy contribution plays a significant role in stabilizing these complexes. The maximum dispersion energy contribution was observed for the

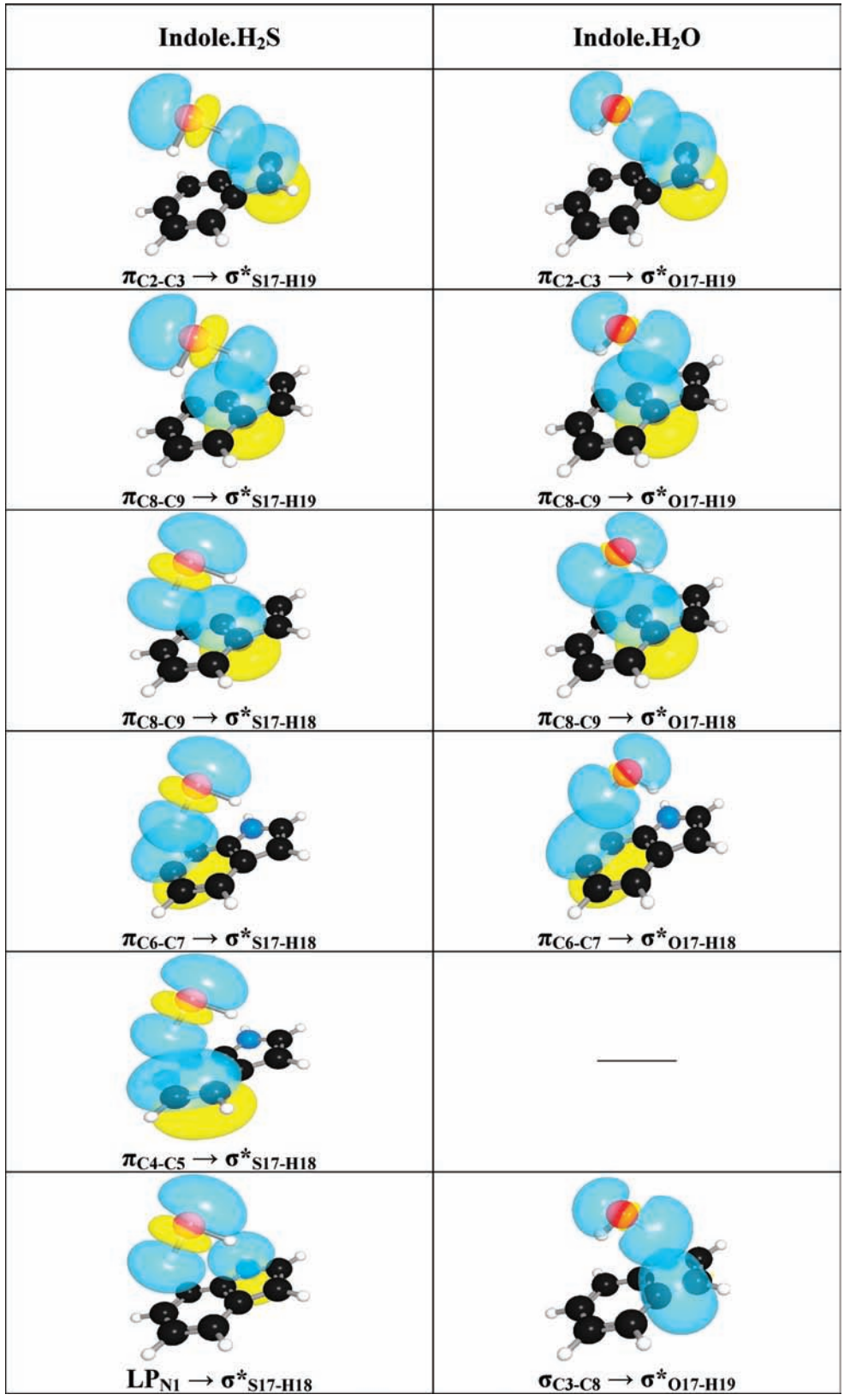

Figure 9. The interacting donor−acceptor natural bond orbitals (NBOs) of IND·H_2S (on left) and IND·H_2O (on right) complexes.

IND·H_2S complex. For rest of them, the dispersion contribution was in the order $CH_4 > NH_3 > H_2O$, which is the inverse order of electronegativity of the central atom. The net electrostatic components were in the order $H_2O \approx H_2S > NH_3 > CH_4$, which is in the same order as the computed XH red shifts in the case of IND·L complexes and also the experimental data for the benzene·L complexes. This suggests that the stabilization energy of X−H···π HB complexes mainly comes from the dispersion contribution, while the magnitude of red shift of the X−H stretch depends on the electrostatic and charge-transfer components. A similar distribution of the energy components has also been reported for the benzene·H_2O, benzene·NH_3, and benzene·CH_4 complexes using a very high level of calculation [CCSD(T) basis set limit].[16]

TABLE 5: Summary of the NBO Analysis for IND·L (X−H···π Hydrogen-Bonded) Complexes (L = H_2O, H_2S, NH_3, and CH_4)

NBO analysis			
donor orbital	acceptor orbital	$E^{(2)}_{i\rightarrow j}$ (kcal/mol)	total interaction energy (kcal/mol)[a]
		Indole·H_2S	
π_{C2-C3}	$\sigma^*_{S17-H19}$	2.10	3.85 (4.89)
π_{C8-C9}	$\sigma^*_{S17-H19}$	0.29	
π_{C6-C7}	$\sigma^*_{S17-H18}$	0.96	
π_{C4-C5}	$\sigma^*_{S17-H18}$	0.31	
π_{C8-C9}	$\sigma^*_{S17-H18}$	0.14	
LP_{N1}	$\sigma^*_{S17-H18}$	0.05	
		Indole·H_2O	
π_{C2-C3}	$\sigma^*_{O17-H19}$	1.53	2.24 (3.57)
π_{C8-C9}	$\sigma^*_{O17-H19}$	0.29	
σ_{C3-C8}	$\sigma^*_{O17-H19}$	0.07	
π_{C8-C9}	$\sigma^*_{O17-H18}$	0.21	
π_{C6-C7}	$\sigma^*_{O17-H18}$	0.14	
		Indole·NH_3	
π_{C2-C3}	$\sigma^*_{N17-H19}$	0.50	1.53 (2.56)
π_{C8-C9}	$\sigma^*_{N17-H19}$	0.21	
π_{C4-C5}	$\sigma^*_{N17-H18}$	0.35	
π_{C6-C7}	$\sigma^*_{N17-H18}$	0.29	
π_{C8-C9}	$\sigma^*_{N17-H18}$	0.11	
$\sigma_{N17-H19}$	π^*_{C8-C9}	0.07	
		Indole·CH_4	
π_{C2-C3}	$\sigma^*_{C17-H21}$	0.69	1.50 (2.01)
π_{C4-C5}	$\sigma^*_{C17-H18}$	0.42	
π_{C6-C7}	$\sigma^*_{C17-H18}$	0.15	
π_{C8-C9}	$\sigma^*_{C17-H20}$	0.24	

[a] Sum total of the second-order perturbative energy $E^{(2)}_{i\rightarrow j^*}$. The values in the parentheses give the binding energies of the complexes computed at the complete basis set limit. For the atom numbering, see Figure 1.

In the σ-type X−H···Y hydrogen bond, the conventional interaction is between the lone pair on the Y atom and the antibonding orbital (σ^*_{X-H}) of the X−H bond. In certain blue-shifted hydrogen bonds (CH···Y type), it has been proposed that the electron density from Y is transferred to the remote parts of the hydrogen-bond-donating molecule.[23−25] However, it is not so straightforward to predict the orbitals participating in the π-type hydrogen bond. The NBO analysis was used to find out the π-orbitals of the electron-rich moiety that overlap with the σ^*_{X-H} orbital. The charge delocalization energy was evaluated as the second-order perturbative energy $E^{(2)}_{i\rightarrow j^*}$, where i and j* denote the interacting donor and the acceptor orbitals, respectively. The strength of hydrogen bond depends directly on the second-order perturbative energy, $E^{(2)}_{i\rightarrow j^*}$, which is proportional to the extent of overlap between the donor and acceptor orbitals.[66−68] The interacting natural bond orbitals for IND·H_2S and IND·H_2O complexes are depicted in Figure 9, and the NBO interaction energies and the involved X−H bond orbitals for all of the π-type IND·L complexes are listed in Table 5. From Figure 9, it can be seen that for both the H_2S and H_2O complexes, both of the XH bonds are interacting with some or the other π orbitals. The strongest interaction in both cases was between the σ^*_{XH} orbital of the XH bond leaning over the pyrole ring and the C_2-C_3 π orbital (for atom numbering, refer to Figure 1). The σ^*_{XH} orbital of the XH bond leaning over the phenyl ring interacts with all three π orbitals, that is, C_4-C_5, C_6-C_7, and C_8-C_9, the interaction with the C_6-C_7 being the strongest. A subtle difference in the IND·H_2O complex was that the π_{C4-C5} was not involved in hydrogen bonding. In all of the complexes, more than one X−H bond were participating in hydrogen bonding. The sum total of the second-order perturbative energy, $E^{(2)}_{i\rightarrow j^*}$ for the IND·H_2S complex was the highest (3.85 kcal/mol), followed by the IND·H_2O (2.24 kcal/mol), IND·NH_3 (1.53 kcal/mol), and IND·CH_4 (1.50 kcal/mol) complexes. The same order was also observed for the computed binding energy of the complexes.

5. Conclusions

S−H···π hydrogen-bonded complexes of H_2S with indole and 3-methylindole were reported for the first time. Experimental data such as band origin shifts and IR spectroscopic and lifetime data give conclusive evidence of the S−H···π type hydrogen bond in these systems. The binding energy was estimated for both the N−H···S σ-type and S−H···π hydrogen-bonded complexes of H_2S using the MP2/CBS level of computation. It shows that the S−H···π HB is much stronger than the N−H···S σ-type HB complex, whereas in the case of the indole·H_2O complex, the O−H···π HB is weaker than the N−H···O σ-type HB complex. This is in complete agreement with the experimental observations that in the case of indole·H_2S, the π-type HB complex (HB donor) is preferentially populated, whereas in the case of indole·H_2O, it is the N−H···S σ-type complex.

Comparison of the S−H···π interaction with the other type of X−H···π (X = C, N, and O) shows that the S−H···π interaction is the strongest among them. The red shift of the S−H stretch is comparable to that of the O−H stretch. Energy decomposition analysis indicates that in all of the π-type HB complexes, the dispersion energy component has significant contribution to the total binding energy. A higher stabilization energy of the H_2S complex and a comparable red shift of the S−H stretch to that of O−H···π HB complex indicates that the total stabilization energy of the X−H···π HB is due to both the dispersion and electrostatic contributions, while the magnitude of the red shift of the X−H stretch depends on the electrostatic and charge-transfer energy components.

At this point, it is worth mulling over a question, what does one call these complexes which are stabilized entirely due to the dispersion interaction but do involve a hydrogen atom covalently bound to one atom and that interacts with another atom or group of atoms which are rich in electron density. They could simply be called hydrogen bonds as they satisfy the primary definition of the hydrogen bond, or alternatively, one could create a new class of hydrogen bonds called dispersion-stabilized hydrogen bonds.

References and Notes

(1) Suzuki, S.; Green, P. G.; Bumgarner, R. E.; Dasgupta, S.; Goddard, W. A.; Blake, G. A. *Science* **1992**, *257*, 942.
(2) Gotch, A. J.; Zwier, T. S. *J. Chem. Phys.* **1992**, *96*, 3388.
(3) Gutowsky, H. S.; Emilsson, T.; Arunan, E. *J. Chem. Phys.* **1993**, *99*, 4883.
(4) Cheng, B. M.; Grover, J. R.; Walters, E. A. *Chem. Phys. Lett.* **1995**, *232*, 364.
(5) Pribble, R. N.; Zwier, T. S. *Faraday Discuss.* **1994**, *97*, 229.
(6) Rodham, D. A.; Suzuki, S.; Suenram, R. D.; Lovas, F. J.; Dasgupta, S.; Goddard, W. A.; Blake, G. A. *Nature* **1993**, *362*, 735.
(7) Weyers, K.; Freudenberg, T.; Ritze, H. H.; Radloff, W.; Stert, V. *Z. Phys. D* **1997**, *39*, 217.
(8) Gotch, A. J.; Zwier, T. S. *J. Chem. Phys.* **1990**, *93*, 6977.
(9) Gotch, A. J.; Pribble, R. N.; Ensminger, F. A.; Zwier, T. S. *Laser Chem.* **1994**, *13*, 187.
(10) Braun, J. E.; Grebner, T. L.; Neusser, H. J. *J. Phys. Chem. A* **1998**, *102*, 3273.
(11) George C. Pimentel, A. L. M. *The hydrogen bond*; W. H. Freeman & Co Ltd.: San Francisco, CA, 1960.
(12) Pribble, R. N.; Garrett, A. W.; Haber, K.; Zwier, T. S. *J. Chem. Phys.* **1995**, *103*, 531.
(13) Fredericks, S. Y.; Jordan, K. D.; Zwier, T. S. *J. Phys. Chem.* **1996**, *100*, 7810.

(14) Zwier, T. S. *Annu. Rev. Phys. Chem.* **1996**, *47*, 205.
(15) Courty, A.; Mons, M.; Dimicoli, N.; Piuzzi, F.; Gaigeot, M. P.; Brenner, V.; de Pujo, P.; Millie, P. *J. Phys. Chem. A* **1998**, *102*, 6590.
(16) Tsuzuki, S.; Honda, K.; Uchimaru, T.; Mikami, M.; Tanabe, K. *J. Am. Chem. Soc.* **2000**, *122*, 11450.
(17) Cheney, B. V.; Schulz, M. W.; Cheney, J. *Biochim. Biophys. Acta* **1989**, *996*, 116.
(18) Tarakeshwar, P.; Kim, K. S. *J. Mol. Struct.* **2002**, *615*, 227.
(19) Mons, M.; Dimicoli, I.; Tardivel, B.; Piuzzi, F.; Brenner, V.; Millie, P. *Phys. Chem. Chem. Phys.* **2002**, *4*, 571.
(20) Mons, M.; Dimicoli, I.; Piuzzi, F. *Int. Rev. Phys. Chem.* **2002**, *21*, 101.
(21) Vaupel, S.; Brutschy, B.; Tarakeshwar, P.; Kim, K. S. *J. Am. Chem. Soc.* **2006**, *128*, 5416.
(22) Enkvist, C.; Zhang, Y. K.; Yang, W. T. *Int. J. Quantum Chem.* **2000**, *79*, 325.
(23) Fujii, A.; Shibasaki, K.; Kazama, T.; Itaya, R.; Mikami, N.; Tsuzuki, S. *Phys. Chem. Chem. Phys.* **2008**, *10*, 2836.
(24) Tsuzuki, S.; Honda, K.; Uchimaru, T.; Mikami, M.; Fujii, A. *J. Phys. Chem. A* **2006**, *110*, 10163.
(25) Tsuzuki, S.; Honda, K.; Uchimaru, T.; Mikami, M.; Tanabe, K. *J. Phys. Chem. A* **2002**, *106*, 4423.
(26) Tarakeshwar, P.; Lee, S. J.; Lee, J. Y.; Kim, K. S. *J. Chem. Phys.* **1998**, *108*, 7217.
(27) Walters, E. A.; Grover, J. R.; White, M. G.; Hui, E. T. *J. Phys. Chem.* **1985**, *89*, 3814.
(28) Steed, J. M.; Dixon, T. A.; Klemperer, W. *J. Chem. Phys.* **1979**, *70*, 4940.
(29) Bornsen, K. O.; Selzle, H. L.; Schlag, E. W. *Z. Naturforsch., A: Phys. Sci.* **1984**, *39*, 1255.
(30) Nishiyama, I.; Hanazaki, I. *Chem. Phys. Lett.* **1985**, *117*, 99.
(31) Grover, J. R.; Walters, E. A.; Hui, E. T. *J. Phys. Chem.* **1987**, *91*, 3233.
(32) Page, R. H.; Shen, Y. R.; Lee, Y. T. *J. Chem. Phys.* **1988**, *88*, 4621.
(33) Selzle, H. L.; Neusser, H. J.; Ernstberger, B.; Krause, H.; Schlag, E. W. *J. Phys. Chem.* **1989**, *93*, 7535.
(34) Jorgensen, W. L.; Severance, D. L. *J. Am. Chem. Soc.* **1990**, *112*, 4768.
(35) Arunan, E.; Gutowsky, H. S. *J. Chem. Phys.* **1993**, *98*, 4294.
(36) Chipot, C.; Jaffe, R.; Maigret, B.; Pearlman, D. A.; Kollman, P. A. *J. Am. Chem. Soc.* **1996**, *118*, 11217.
(37) Hobza, P.; Selzle, H. L.; Schlag, E. W. *J. Phys. Chem.* **1996**, *100*, 18790.
(38) Hobza, P.; Spirko, V.; Selzle, H. L.; Schlag, E. W. *J. Phys. Chem. A* **1998**, *102*, 2501.
(39) Sinnokrot, M. O.; Valeev, E. F.; Sherrill, C. D. *J. Am. Chem. Soc.* **2002**, *124*, 10887.
(40) Wang, W. Z.; Pitonak, M.; Hobza, P. *ChemPhysChem* **2007**, *8*, 2107.
(41) Wheeler, S. E.; Houk, K. N. *J. Am. Chem. Soc.* **2008**, *130*, 10854.
(42) Dinadayalane, T. C.; Leszczynski, *J. Struct. Chem.* **2009**, *20*, 11.
(43) Arunan, E.; Emilsson, T.; Gutowsky, H. S.; Fraser, G. T.; de Oliveira, G.; Dykstra, C. E. *J. Chem. Phys.* **2002**, *117*, 9766.
(44) Morgan, R. S.; Tatsch, C. E.; Gushard, R. H.; McAdon, J. M.; Warme, P. K. *Int. J. Pept. Protein Res.* **1978**, *11*, 209.
(45) Reid, K. S. C.; Lindley, P. F.; Thornton, J. M. *FEBS Lett.* **1985**, *190*, 209.
(46) Duan, G. L.; Smith, V. H.; Weaver, D. F. *Mol. Phys.* **2001**, *99*, 1689.
(47) Iwaoka, M.; Takemoto, S.; Okada, M.; Tomoda, S. *Bull. Chem. Soc. Jpn.* **2002**, *75*, 1611.
(48) Meyer, E. A.; Castellano, R. K.; Diederich, F. *Angew. Chem., Int. Ed.* **2003**, *42*, 1210.
(49) Cerny, J.; Hobza, P. *Phys. Chem. Chem. Phys.* **2007**, *9*, 5291.
(50) Hermida-Ramon, J. M.; Cabaleiro-Lago, E. M.; Rodriguez-Otero, J. *J. Chem. Phys.* **2005**, *122*, 204315.
(51) Tauer, T. P.; Derrick, M. E.; Sherrill, C. D. *J. Phys. Chem. A* **2005**, *109*, 191.
(52) Ringer, A. L.; Senenko, A.; Sherrill, C. D. *Protein Sci.* **2007**, *16*, 2216.
(53) Cabaleiro-Lago, E. M.; Rodriguez-Otero, J.; Pena-Gallego, A. *J. Phys. Chem. A* **2008**, *112*, 6344.
(54) Cabaleiro-Lago, E. M.; Rodriguez-Otero, J.; Pena-Gallego, A. *J. Chem. Phys.* **2008**, *129*, 084305.
(55) Biswal, H. S.; Shirhatti, P. R.; Wategaonkar, S. *J. Phys. Chem. A* **2009**, *113*, 5633.
(56) Demmer, D. R.; Leach, G. W.; Wallace, S. C. *J. Phys. Chem.* **1994**, *98*, 12834.
(57) Carney, J. R.; Zwier, T. S. *J. Phys. Chem. A* **1999**, *103*, 9943.
(58) Dian, B. C.; Longarte, A.; Zwier, T. S. *J. Chem. Phys.* **2003**, *118*, 2696.
(59) Georgiev, S.; Neusser, H. J. *Chem. Phys. Lett.* **2004**, *389*, 24.
(60) Mons, M.; Dimicoli, I.; Tardivel, B.; Piuzzi, F.; Brenner, V.; Millie, P. *J. Phys. Chem. A* **1999**, *103*, 9958.
(61) Meenakshi, P. S.; Biswas, N.; Wategaonkar, S. *J. Chem. Phys.* **2002**, *117*, 11146.
(62) Biswal, H. S.; Chakraborty, S.; Wategaonkar, S. *J. Chem. Phys.* **2008**, *129*, 184311.
(63) Frisch, M. J.; Trucks, G. W.; Schlegel, H. B.; Scuseria, G. E.; Robb, M. A.; Cheeseman, J. R.; Montgomery, J. A., Jr.; Vreven, T.; Kudin, K. N.; Burant, J. C.; Millam, J. M.; Iyengar, S. S.; Tomasi, J.; Barone, V.; Mennucci, B.; Cossi, M.; Scalmani, G.; Rega, N.; Petersson, G. A.; Nakatsuji, H.; Hada, M.; Ehara, M.; Toyota, K.; Fukuda, R.; Hasegawa, J.; Ishida, M.; Nakajima, T.; Honda, Y.; Kitao, O.; Nakai, H.; Klene, M.; Li, X.; Knox, J. E.; Hratchian, H. P.; Cross, J. B.; Bakken, V.; Adamo, C.; Jaramillo, J.; Gomperts, R.; Stratmann, R. E.; Yazyev, O.; Austin, A. J.; Cammi, R.; Pomelli, C.; Ochterski, J. W.; Ayala, P. Y.; Morokuma, K.; Voth, G. A.; Salvador, P.; Dannenberg, J. J.; Zakrzewski, V. G.; Dapprich, S.; Daniels, A. D.; Strain, M. C.; Farkas, O.; Malick, D. K.; Rabuck, A. D.; Raghavachari, K.; Foresman, J. B.; Ortiz, J. V.; Cui, Q.; Baboul, A. G.; Clifford, S.; Cioslowski, J.; Stefanov, B. B.; Liu, G.; Liashenko, A.; Piskorz, P.; Komaromi, I.; Martin, R. L.; Fox, D. J.; Keith, T.; Al-Laham, M. A.; Peng, C. Y.; Nanayakkara, A.; Challacombe, M.; Gill, P. M. W.; Johnson, B.; Chen, W.; Wong, M. W.; Gonzalez, C.; Pople, J. A. *Gaussian 03*, revision D.1; Gaussian, Inc.: Wallingford, CT, 2005.
(64) ChemCraft. Website: http://www.softpedia.com/progDownload/ChemCraft-Download-56007.html.
(65) Helgaker, T.; Klopper, W.; Koch, H.; Noga, J. *J. Chem. Phys.* **1997**, *106*, 9639.
(66) Weinhold, F. In *Encyclopedia of Computational Chemistry*; Schleyer, P. v. R., Allinger, N. L., Gasteiger, T., Clark, J., Kollman, P. A., Schaefer, H. F. S., III, Schreiner, P. R., Eds.; John Wiley & Sons: Chichester, U.K., 1998; Vol. 3; p 1792.
(67) Weinhold, F.; Landis, C. R. *Chem. Educ. Res. Pract. Eur.* **2001**, *2*, 91.
(68) Weinhold, F.; Landis, C. R. *Valency and Bonding: A Natural Bond Orbital Donor-Acceptor Perspective*; Cambridge University Press: New York, 2005.
(69) *NBO 5.0.*; Glendening, J., Badenhoop, K., Reed, A. E., Carpenter, J. E., Bohmann, J. A., Morales, C. M., Weinhold, F., Eds.; Theoretical Chemistry Institute, University of Wisconsin: Madison, WI, 2001.
(70) Chalasinski, G.; Szczesniak, M. M. *Chem. Rev.* **2000**, *100*, 4227.
(71) Stevens, W. J.; Fink, W. H. *Chem. Phys. Lett.* **1987**, *139*, 15.
(72) Chen, W.; Gordon, M. S. *J. Phys. Chem.* **1996**, *100*, 14316.
(73) Schmidt, M. W.; Baldridge, K. K.; Boatz, J. A.; Elbert, S. T.; Gordon, M. S.; Jensen, J. H.; Koseki, S.; Matsunaga, N.; Nguyen, K. A.; Su, S. J.; Windus, T. L.; Dupuis, M.; Montgomery, J. A. *J. Comput. Chem.* **1993**, *14*, 1347.
(74) NIST Computational Chemistry Comparison and Benchmark DataBase; NIST: Gaithersburg, MD, http://cccbdb.nist.gov.
(75) Braun, J. E.; Mehnert, T.; Neusser, H. J. *Int. J. Mass Spectrom.* **2000**, *203*, 1.
(76) Hager, J.; Wallace, S. C. *J. Phys. Chem.* **1983**, *87*, 2121.
(77) Lechugafossat, L.; Flaud, J. M.; Camypeyret, C.; Johns, J. W. C. *Can. J. Phys.* **1984**, *62*, 1889.
(78) Tsujii, H.; Takizawa, K.; Koda, S. *Chem. Phys.* **2002**, *285*, 319.
(79) Unpublished results.
(80) Montoro, T.; Jouvet, C.; Lopez-Campillo, A.; Soep, B. *J. Phys. Chem.* **1983**, *87*, 3582.
(81) Nibu, Y.; Abe, H.; Mikami, N.; Ito, M. *J. Phys. Chem.* **1983**, *87*, 3898.
(82) Cable, J. R. *J. Chem. Phys.* **1990**, *92*, 1627.
(83) Short, K. W.; Callis, P. R. *J. Chem. Phys.* **2000**, *113*, 5235.
(84) Sobolewski, A. L.; Domcke, W.; Dedonder-Lardeux, C.; Jouvet, C. *Phys. Chem. Chem. Phys.* **2002**, *4*, 1093.
(85) Braun, J.; Neusser, H. J.; Hobza, P. *J. Phys. Chem. A* **2003**, *107*, 3918.
(86) Somers, K. R. F.; Ceulemans, A. *J. Phys. Chem. A* **2004**, *108*, 7577.
(87) Georgiev, S.; Neusser, H. J. *J. Electron Spectrosc. Relat. Phenom.* **2005**, *142*, 207.
(88) David, O.; Dedonder-Lardeux, C.; Jouvet, C.; Sobolewski, A. L. *J. Phys. Chem. A* **2006**, *110*, 9383.
(89) Sukhodola, A. A. *J. Appl. Spectrosc.* **2008**, *75*, 527.
(90) Hager, J.; Wallace, S. C. *J. Phys. Chem.* **1984**, *88*, 5513.
(91) Hager, J.; Wallace, S. C. *Can. J. Chem.* **1985**, *63*, 1502.
(92) Hager, J. W.; Demmer, D. R.; Wallace, S. C. *J. Phys. Chem.* **1987**, *91*, 1375.
(93) Demmer, D. R.; Leach, G. W.; Outhouse, E. A.; Hager, J. W.; Wallace, S. C. *J. Phys. Chem.* **1990**, *94*, 582.
(94) Arnold, S.; Sulkes, M. *J. Phys. Chem.* **1992**, *96*, 4768.
(95) Morita, S.; Fujii, A.; Mikami, N.; Tsuzuki, S. *J. Phys. Chem. A* **2006**, *110*, 10583.
(96) Shibasaki, K.; Fujii, A.; Mikami, N.; Tsuzuki, S. *J. Phys. Chem. A* **2006**, *110*, 4397.
(97) Crittenden, D. L. *J. Phys. Chem. A* **2009**, *113*, 1663.

JP907747W